Vibrational modes of oxygen in GaP including nearest-neighbor interactions

R. M. Feenstra,* R. J. Hauenstein, and T. C. McGill
California Institute of Technology, Pasadena, California 91125
(Received 10 March 1983; revised manuscript received 16 August 1983)

A theoretical treatment of the vibrational modes of substitutional defects in zinc-blende crystals is presented. The dynamics of the perfect lattice are described with the use of a two-parameter model including nearest-neighbor interactions only. The defect consists of an impurity atom with variable strength nearest-neighbor force constants. For the case of oxygen in GaP, the theoretical defect vibrational modes are compared with experiment. Agreement between theory and experiment is obtained for values of the defect force constants which are 15% of the bulk values for the O^0 and O^+ defects, indicating that the oxygen impurity is quite weakly bonded in the lattice.

I. INTRODUCTION

An oxygen atom on a P site in GaP is a defect with many interesting and controversial properties. The vibrational states of the defect are observed in phonon-assisted transitions appearing in a variety of optical spectra.[1-4] From the relatively low energy of those phonon modes which involve oxygen motion,[2] it seems that the oxygen impurity is quite weakly bonded in the lattice,[5] and recent theoretical studies[6] support this conclusion. In this paper, we theoretically examine the vibrational modes of an oxygen defect with T_d symmetry. We use a phenomenological model for the lattice dynamics with the force constants between the defect and neighboring atoms being treated as parameters in the theory. We compare our results with experiment for the O^0 and O^+ defects (with and without the first donor electron present, respectively). We find reasonable agreement between theory and experiment for defect force constants which are about 15% of the bulk values, thus supporting the current view that the O^0 and O^+ defects are weakly bonded in a T_d symmetric site.

In this paper the dynamics of the perfect lattice are described using a two-parameter model which includes nearest-neighbor interactions only. By symmetry, only two parameters are required for the most general description of the bulk phonons in this model,[7] and these parameters are chosen to fit known phonon dispersion curves. A substitutional defect consists of an impurity atom of given mass with variable-strength nearest-neighbor force constants. The properties of a defect are thus determined by only two parameters. Therefore, we are able to obtain quite general results for defects within our very simplified model for the bulk crystal. More complicated models are available for the bulk phonons, and, in particular, the 15-parameter deformable-dipole model of Kunc[8] seems to give a good description of many III-V compounds. However, within this model a substitutional defect is also described by 15 (or more) parameters, and the results for the defect vibrational modes may be somewhat dependent on the choice of parameter values. Thus, the complicated models yield specific results for a defect within a realistic model for the bulk. Because of this phenomenological nature of our calculations we feel that it is necessary to examine the results from both the simple and complicated dynamical models. In this paper we present results from the simple two-parameter model and results from the deformable-dipole model are planned to be the topic of a forthcoming publication.[9]

Previous workers[5,6,10] have considered the vibrational states of the GaP:O defect using molecular-type models of the defect and its immediate neighbors. Here, we use the Green's-function technique,[11] which allows us to compute the vibrational states of the defect including the response of the entire lattice. The advantage of this technique is that it allows us to couple the vibrations of the defect into the bulk crystal and see which types of vibrational modes remain localized around the defect. The term "localized" will be used here to refer to both strictly localized vibrational modes and resonant vibrational modes in which the vibrational amplitude is relatively peaked near the defect. The quantity we will use to describe the vibrational modes of a defect is the local density of states (LDOS). Strictly localized modes show up as δ functions in the LDOS and resonant modes appear as peaks with some nonzero width.

In Sec. II we present the details of our computational technique. Our method is quite similar to other vibrational Green's-function computations.[7,12] The results of our calculations are presented in Sec. III. We show the computed dispersion curves and density of states (DOS) for the bulk phonons in GaP. A model is used for the substitutional O defect in which the nearest-neighbor O-Ga force constants are all varied by the same amount. For various values of the defect force constant the LDOS for A_1 and T_2 defect vibrational modes are presented. We find basically one A_1 and one T_2 vibrational mode of the defect. In Sec. IV we compare our theoretical results with experiment. For defect force constants which are 15% of the bulk values, we identify our computed T_2 mode with the 24.7-meV resonance observed for the O^0 defect.[2] Our computed A_1 mode is identified with the 19-meV mode observed,[1,3] for the O^0 and O^+ defects. We argue that these phonons are the most localized models of the defect. Other modes observed in the optical spectra are either bulklike phonons or relatively delocalized defect modes. The conclusions which can be drawn from this work are presented in Sec. V.

II. COMPUTATIONAL METHOD

A. Bulk phonons

The lattice dynamics of the perfect crystal are described using a two-parameter model consisting of nearest-neighbor interactions only. As shown by Grimm *et al.*,[7] in the harmonic approximation, invariance of potential energy with respect to rigid-body translations, rotations, and symmetry operations of the crystal lattice result in only two parameters required to describe the bulk phonons. In this model the matrix of second derivatives of the potential energy with respect to atomic positions has diagonal Cartesian blocks of the form

$$\Phi(\mathrm{Ga};\mathrm{Ga})=\Phi(\mathrm{P};\mathrm{P})=\begin{bmatrix}4A & 0 & 0\\ 0 & 4A & 0\\ 0 & 0 & 4A\end{bmatrix} \tag{1a}$$

and off-diagonal blocks typically of the form

$$\Phi(\mathrm{Ga};\mathrm{P})=\Phi(\mathrm{P};\mathrm{Ga})=-\begin{bmatrix}A & B & B\\ B & A & B\\ B & B & A\end{bmatrix} . \tag{1b}$$

For convenience we decompose the parameters A and B into bond-stretching and bond-bending components.[13] The contribution to the potential energy of the system from a bond (spring) connecting atoms i and j is written as

$$V=\tfrac{1}{2}f_1\,|\,(\vec{u}_i-\vec{u}_j)\cdot\hat{e}_{ij}\,|^2+\tfrac{1}{2}f_2\,|\,(\vec{u}_i-\vec{u}_j)\times\hat{e}_{ij}\,|^2 , \tag{2a}$$

with

$$\hat{e}_{ij}=\frac{\vec{R}_i-\vec{R}_j}{|\,\vec{R}_i-\vec{R}_j\,|} \tag{2b}$$

where $\vec{u}_i$ is the displacement of the ith atom from its equilibrium position $\vec{R}_i$. The parameters f_1 and f_2 are defined as bond-stretching and bond-bending force constants, respectively, and are related to A and B by $A=(f_1+2f_2)/3$ and $B=(f_1-f_2)/3$.

B. Green's functions

From the eigenvalues and eigenvectors of the dynamical matrix we compute the perfect crystal Green's function G^0. Maradudin[11] has shown that the matrix elements of G^0 can be expressed as

$$G^{0\alpha\beta}_{lmab}(\omega^2)=\frac{1}{N\sqrt{m_a m_b}}\lim_{\epsilon\to 0^+}\sum_{n,\vec{k}}\frac{\xi^{\alpha}_a(n,\vec{k})\xi^{\beta *}_b(n,\vec{k})\exp[i\vec{k}\cdot(\vec{R}_{la}-\vec{R}_{mb})]}{\omega^2+i\epsilon-\omega^2_{n,\vec{k}}} , \tag{3}$$

where l and m label the N unit cells, a and b label atomic types, and α and β label Cartesian coordinates. $\omega^2_{n,\vec{k}}$ are the eigenvalues and $\xi^{\alpha}_a(n,\vec{k})$ are the eigenvectors of the $(n,\vec{k})$th normal mode. The equilibrium position of an atom is denoted by $\vec{R}_{la}$, and m_a is the mass of the ath atom.

To evaluate the LDOS of a crystal containing a defect it is necessary to compute that portion of the Green's function which is in the space of the defect. The defects we consider here consist of a substitutional impurity atom in a zinc-blende crystal with bonds of variable strength connecting the impurity atom to its neighboring atoms. This defect consists of a five-atom cluster with T_d symmetry. The positions of the five atoms are specified by 15 Cartesian coordinates, which form a 15-dimensional representation of the T_d group. This reducible representation Γ can be decomposed into the irreducible representation of the T_d group according to

$$\Gamma=A_1+E+T_1+3T_2 . \tag{4}$$

This equation classifies the collective coordinates of the five-atom cluster. The A_1 coordinate consists of a "breathing" type of motion in which the central atom is stationary and the outer atoms move radially. The motion of the central impurity atom forms a basis for a T_2 representation of the T_d group. The other two sets of T_2 coordinates involve motion of the outer atoms. Similarly, the E and T_1 coordinates involve motion of the outer atoms with the inner atom stationary. The definition of all the collective coordinates is given in Appendix A.

To produce a Green's function suitable for computation we apply two coordinate transformations. The first transformation is quite trivial and its effect is to drop the masses m_a and m_b from Eq. (3) and to absorb them into the defect perturbation matrix δL. This corresponds to expressing G^0 with respect to the reduced coordinates $q_i=\sqrt{m_i}\,u_i$ where u_i are Cartesian coordinates. Secondly, we transform to the collective coordinates Q_i defined in Appendix A. In this coordinate system (s) and (r) label the irreducible representation, σ and ρ label the occurrence of the representation, and μ and ν label the row or column of the representation. The Green's function in the space of the defect can now be expressed as

$$G^{0\mu\nu}_{(s)(r)\sigma\rho}(\omega^2)=\frac{1}{N}\lim_{\epsilon\to 0^+}\sum_{n,\vec{k}}\frac{Q^{\mu}_{(s)\sigma}(n,\vec{k})Q^{\nu *}_{(r)\rho}(n,\vec{k})}{\omega^2+i\epsilon-\omega^2_{n,\vec{k}}} . \tag{5}$$

The summation on $\vec{k}$ extends over the entire first Brillouin zone. This can be divided into a sum over the irreducible wedge W of the zone and a sum over the group elements R which define the star of $\vec{k}$. Since the Q coordinates form bases for irreducible representations of the T_d group, they are orthogonal when summed over R, and we find that

$$G^{0\mu\nu}_{(s)(r)\sigma\rho}(\omega^2)=\frac{1}{N}\lim_{\epsilon\to 0^+}\sum_{n,\vec{k}\in W}\delta_{\mu\nu}\delta_{(s)(r)}\frac{h_{\vec{k}}}{d_s}\frac{\mathrm{Re}\left[\sum_{\kappa}Q^{\kappa}_{(s)\sigma}(n,\vec{k})Q^{\kappa *}_{(r)\rho}(n,\vec{k})\right]}{\omega^2+i\epsilon-\omega^2_{n,\vec{k}}}\,, \tag{6}$$

where $h_{\vec{k}}$ is the number of points in the star of $\vec{k}$ and d_s is the dimension of the representation (s) [compare with Eq. (41) of Ref. 14]. We see that the Green's function is zero unless $(s)=(r)$ and $\mu=\nu$, in which case it is independent of μ. Thus the Green's function has been block-diagonalized by the transformation to the collective coordinates. The transformed matrix consists of 1×1, 2×2, 3×3, and 9×9 blocks for the A_1, E, T_1, and $3T_2$ representations, respectively. Furthermore, these matrix elements do not depend on the row or column of the representation, so that these blocks can be further reduced to 1×1, 1×1, 1×1, and 3×3 symmetric blocks, respectively, for a total of nine independent matrix elements. Keeping the zero elements in mind we can simplify the notation by dropping the subscripts μ, ν, and (r). Furthermore, the Green's function can be explicitly divided into its real and imaginary parts by defining the partial DOS ("spectral density"),

$$D_{(s)\sigma\rho}(\omega^2)=\frac{1}{N}\sum_{n,\vec{k}\in W}\frac{h_{\vec{k}}}{d_s}\mathrm{Re}\left[\sum_{\kappa}Q^{\kappa}_{(s)\sigma}(n,\vec{k})Q^{\kappa *}_{(r)\rho}(n,\vec{k})\right]\times\delta(\omega^2-\omega^2_{n,\vec{k}})\,, \tag{7}$$

from which Eq. (6) can be expressed as[14,15]

$$G^0_{(s)\sigma\rho}(\omega^2)=\mathrm{P}\int_0^{\infty}\frac{D_{(s)\sigma\rho}(\bar{\omega}^2)}{\bar{\omega}^2-\omega^2}d\bar{\omega}^2-i\pi D_{(s)\sigma\rho}(\omega^2)\,, \tag{8}$$

where P signifies a principle-value integral. Equations (7) and (8) are in a form suitable for computation. The sum over $\vec{k}$ (in the first Brillouin zone) was reduced to a sum over the irreducible wedge ($\frac{1}{48}$th of the Brillouin zone for the zinc-blende structure) and was performed using the Gilat-Raubenheimer method.[16,17] The principal-value integral was then computed following Bernholc and Pantelides.[15] The results presented here were computed using 5950 points in the irreducible wedge corresponding to 256 000 points in the entire zone. The computations were all performed as a function of ω^2, using an interval size of 4.12 meV^2. This corresponds to an accuracy of about 0.05 meV in the optical branches and 0.5 meV near the bottom of the acoustic branch. The number of points used in the $\vec{k}$-space summation was consistent with this ω^2 interval size. For plotting purposes the Green's functions were converted to a linear energy scale by

$$\tilde{G}(\omega)d\omega=G(\omega^2)d\omega^2\,, \tag{9}$$

where $\tilde{G}$ are the functions which will be shown here.

The Green's function for the imperfect crystal in the space of the defect is computed from[11]

$$G=(1-G^0\delta L)^{-1}G^0\,, \tag{10}$$

where G^0 and δL are, respectively, the Green's-function and defect-perturbation matrices in the 15×15 space of the defect. The diagonal elements of $-\mathrm{Im}G/\pi$ give the LDOS of the imperfect crystal. For representations which have multiple occurrences in the space of the defect, the LDOS for each occurrence provides a measure of the fraction of total kinetic energy in that particular type of motion, and this quantity is used in the following sections to describe the composition of the T_2 defect modes.

C. Defect-perturbation matrix

The defect-perturbation matrix δL is defined by[11]

$$\delta L=-\omega^2\Delta M+\Delta\Phi\,, \tag{11}$$

where ΔM and $\Delta\Phi$ are, respectively, the mass-defect and force-constant-defect matrices. As discussed by Maradudin,[11] $\Delta\Phi$ must be invariant under rigid-body translations, rotations, and the symmetry operations of the imperfect crystal. In the present model, assuming the same value of the force constants change ΔA and ΔB for each of the four bonds surrounding the mass defect, the defect-perturbation matrix has the form given by Talwar, Vandevyver, and Zigone (Table 2 of Ref. 12). The $\Delta\Phi$ component of this matrix explicitly satisfies invariance with respect to translations and crystal symmetry operations. To further satisfy rotational invariance it is necessary to assign $\Delta A=\Delta B$ ($At=Bt$ in the notation of Ref. 12), or equivalently the change in bond bending must be zero, $\Delta f_2=0$. The physical origin of such a constraint is as follows: Bond bending clearly violates rotational invariance for an isolated XY_4 molecule in space since a rotation of the molecule produces a nonzero energy change, and the invariance constraints for such an isolated molecule are identical with those for the "defect molecule" considered here. However, in considering very weakly bonded defects one would like to uniformly reduce both the bond-stretching and bond-bending force constants to zero to produce a defect which experiences zero restoring force (i.e., $\Delta f_1/f_1=\Delta f_2/f_2\to-1$ or equivalently $\Delta A/A=\Delta B/B\to-1$). In order to arbitrarily vary the bond-bending force constant it is necessary to introduce an additional defect force constant which has the form of a second-nearest-neighbor bond-bending interaction [as defined in Eq. (2a)] among the four atoms surrounding the mass defect. Denoting this force constant by μ, rotational invariance is satisfied by the condition $\mu=-\Delta f_2/4$. The final form of the defect perturbation matrix is given in Appendix B. We note that the constraint of rotational invariance affects our results only through bond-bending interactions which are relatively small for the GaP lattice. In a preliminary report[18] of our results we neglected rotational invariance, and a comparison between those results

and the results to be presented here reveals that the effects of rotational invariance condition are indeed negligible. Nevertheless, rotational invariance is a fundamental property of the system, and in this paper we completely include its effects.

III. RESULTS

A. Bulk phonons

Shown in Fig. 1 are phonon dispersion curves and DOS computed from the two-parameter model described in Sec. II A. The values of the model parameters f_1 and f_2 have been chosen to produce a reasonable fit to the actual phonon energies of GaP, by matching the TA_X and TO_Γ energies. From the dynamical matrix given by Grimm *et al.*[7] these energies are found to be

$$\omega^2(\mathrm{TO}_\Gamma)=\frac{4A}{M} \tag{12a}$$

and

$$\omega^2(\mathrm{TA}_X)=\frac{4A}{M}\left\{\frac{1}{2}-\frac{1}{2}\left[1-\frac{4M}{m_a+m_b}\left[1-\frac{B^2}{A^2}\right]\right]^{1/2}\right\}, \tag{12b}$$

where A and B are specified in Eq. (1) and $M=m_a m_b/(m_a+m_b)$ with a denoting Ga and b denoting P. For GaP the actual energies are known to be[19] $E(\mathrm{TA}_X)=13.1$ meV and $E(\mathrm{TO}_\Gamma)=45.4$ meV, from which the values for the force constants are determined to be $f_1=6.87$ eV/Å^2 and $f_2=0.525$ eV/Å^2. Our dispersion curves can be compared with the shell-model results of Yarnell *et al.*[20] and the deformable-dipole model results of Kunc.[8] The major deficiency of the present computation is that the LO branch (near 40 meV) should actually be higher in energy due to electrostatic interactions which have been neglected in our model. This may affect our results for defect modes in this branch, but it should have little effect on the defect modes at other energies.

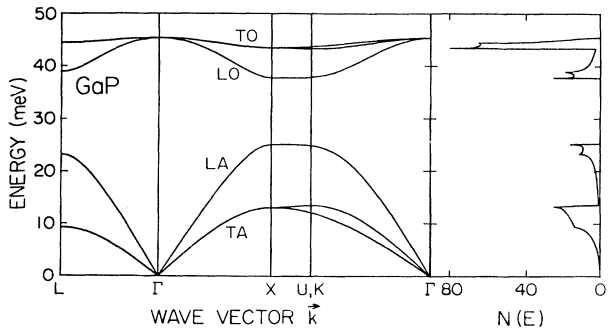

FIG. 1. Phonon dispersion curves and DOS $N(E)$ of GaP computed using the two-parameter valence-force model described in the text. Acoustic (A) and optical (O) branches are labeled according to the polarization of the phonons (T is transverse and L is longitudinal). Some branches may have mixed polarization.

B. Perfect-crystal Green's functions

Shown in Fig. 2 are the elements of the Green's-function matrix for the perfect crystal as computed from Eqs. (6) and (8). These functions are computed using a P site as the origin. We plot $-\mathrm{Im}G^0/\pi$ for the A_1, E, T_1, and the diagonal elements of the T_2 representations. Shown on the top of Fig. 2 is the bulk DOS. The Green's-function elements give the partial DOS for each representation. The appearance of the Green's-function elements may be understood by considering the type of atomic motion they represent. For example, the A_1 Green's function is a breathing motion which is made up entirely from longitudinal phonons. With our P-site origin, the A_1 Green's function is very small in the optical branch because the optical modes involve very little motion of the Ga atoms due to the mass difference between Ga and P. The Ga-site Green's function elements can be obtained from the P-site elements by reflecting the $G(\omega^2)$ functions through a mirror plane located at $\omega^2_{\max}/2$, where $\omega^2_{\max}$ occurs at the top of the optical branch (e.g., the A_1 Ga-site partial DOS has a small peak in the acoustic branch and a large peak in the optical branch). By summing the partial densities for both a P-site origin and a Ga-site origin we obtain the entire DOS,

$$-\frac{1}{\pi}\mathrm{Im}(\mathrm{Tr}G^0_{\mathrm{P}})-\frac{1}{\pi}\mathrm{Im}(\mathrm{Tr}G^0_{\mathrm{Ga}})=5D(\omega^2)\,, \tag{13a}$$

where

$$\mathrm{Tr}G=[G(A_1)+2G(E)+3G(T_1)+3G(T_2^a)+3G(T_2^b)+3G(T_2^c)]\,. \tag{13b}$$

The factor of 5 on the right-hand side of Eq. (13a) arises from the presence of five atoms in the defect cluster. The

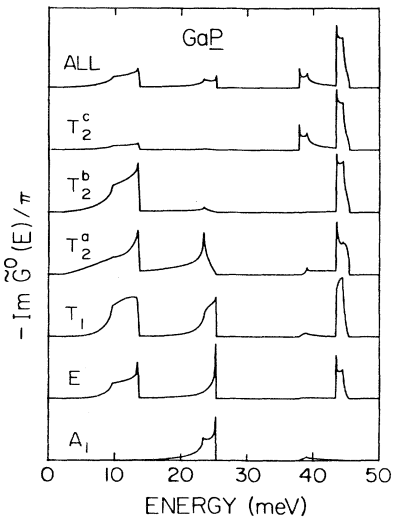

FIG. 2. Imaginary part of the Green's function for the perfect crystal using a P site for the origin in space. At the top is shown the bulk DOS. Elements of the Green's-function matrix shown here are the partial DOS in each of the A_1, E, T_1, T_2^a, T_2^b, and T_2^c CC's.

DOS obtained from Eq. (13) can be compared with that directly computed from

$$D(\omega^2)=\frac{1}{N}\sum_{n,\vec{k}}\delta(\omega^2-\omega^2_{n,\vec{k}}) . \tag{14}$$

In our calculations, the $D(\omega^2)$ computed in these two ways agree to an absolute accuracy of 0.004 (for an energy scale corresponding to $\omega_{\max}=1$), which provides an important check on the computation of the Green's functions.

C. Defect vibrational modes

The vibrational modes of a defect are characterized by a peak in the LDOS. This peak is the center of a band of vibrational modes in which the defect vibrates with significantly greater amplitude than those atoms far removed from it. The defect we are considering consists of an impurity atom substitutional for the P atom. Our results are for oxygen with a mass-defect parameter of

$$\frac{\Delta m}{m}=\frac{m_O-m_P}{m_P}=-0.4834 . \tag{15}$$

The springs which connect the impurity to its nearest neighbors are described by bond-stretching f_1' and bond-bending f_2' interactions. These interactions are allowed to differ from those of the bulk and they are varied by the same fractional amount. Thus the defect-perturbation matrix depends on only one parameter, $\Delta f/f$, the fractional change in spring constants for the defect relative to the bulk material,

$$\frac{\Delta f}{f}=\frac{f_1'-f_1}{f_1}=\frac{f_2'-f_2}{f_2} , \tag{16}$$

where f_1 and f_2 are the bulk spring constants. Negative values of $\Delta f/f$ refer to a weakly bonded defect and positive values refer to a strongly bonded defect. By definition $\Delta f/f\geq -1$. It seems physically unlikely that a substitutional impurity will form bonds which are very much stronger than those of the bulk material. Therefore, we will concentrate our attention on the range $-1<\Delta f/f<1$.

For given values of defect spring constants, we compute the LDOS for each type of vibrational mode (A_1, E, T_1, and T_2). The LDOS reflects some details of the bulk vibrational modes and also has peaks for each of the defect modes. For defect-perturbation values in the range $-1<\Delta f/f<1$ we find defect modes of A_1 and T_2 symmetry only. The A_1 (breathing) mode shown in Fig. 3 is a resonance in the acoustic branch. For $\Delta f/f=0$ the A_1 LDOS curve at the top of the figure is identical to the A_1 Green's function for the perfect crystal. As $\Delta f/f$ is reduced a resonance mode appears and moves to lower energies. This resonance is rather broad, with a width of about 5 meV. The sum of LDOS for the T_2^a, T_2^b and T_2^c modes is shown in Fig. 4. These modes consist of vibrations of the oxygen atom itself along with some response of the rest of the lattice. For $\Delta f/f=0$ we obtain a strictly localized mode at 56.3 meV. As $\Delta f/f$ is reduced this T_2 mode falls in energy, entering the optical branch as a resonance, becoming strictly localized in the acoustic-optical gap, and finally entering the acoustic branch as a rather sharp resonance. As $\Delta f/f\rightarrow -1$, the T_2 mode approaches a δ function at zero energy corresponding to motion of the oxygen atom alone in the absence of any

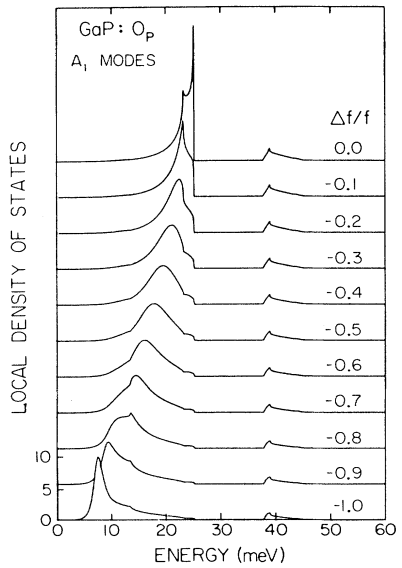

FIG. 3. LDOS of A_1 modes for an O atom on a P site in GaP. Defect force constants $\Delta f/f$ are varied from $\Delta f/f=0$ (defect springs identical to bulk springs) to $\Delta f/f=-1$ (defect springs to zero strength). Resonance in the acoustic branch appears as a peak in the LDOS. This resonance moves to lower energies as the defect force constant is reduced.

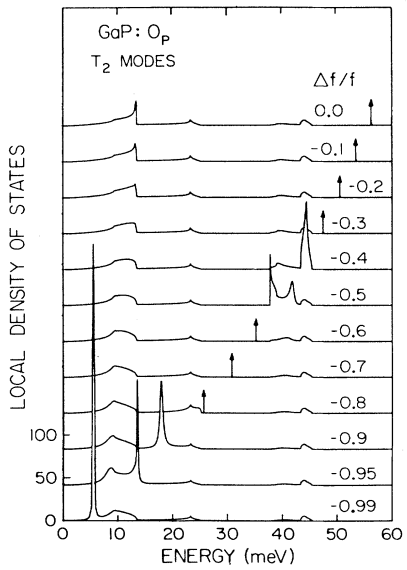

FIG. 4. LDOS of T_2 modes for an O atom on a P site in GaP. For a defect force constant of $\Delta f/f=0$ a strictly localized mode at 56 meV is shown as a δ function in the LDOS. As $\Delta f/f$ is reduced this mode moves to lower energies, entering the optical branch as a resonance, becoming strictly localized in the acoustic-optical gap, and entering the acoustic branch as a sharp resonance.

restoring force. The T_2 resonances in optical and acoustic branches are relatively sharp with a width of less than 2 meV. The T_2-defect modes generally consist of at least 80% O (T_2^c) motion. An exception to this is the strictly localized mode in the energy range 25—30 meV which is typically $0.90T_2^a+0.08T_2^b+0.02T_2^c$ (presumably this mode is comprised largely of bulk phonons from the very top of the LA branch which include very little P-atom motion).

The results from the LDOS calculations are summarized in Fig. 5. Here we plot the energies of the defect modes versus the defect-spring-constant parameter. On the left-hand side of the figure a bulk DOS is shown for reference. The solid lines in the figure are the Green's-function results. These energies are defined as the location of zeros in the real part of the eigenvalues of the matrix $(1-G^0\delta L)$ [Eq. (10)]. For $\Delta f/f<0$ we see the A_1 and T_2 modes discussed above. For $\Delta f/f>0$ another T_2 mode consisting of about 70% T_2^b motion appears as a resonance in the acoustic branch. For $-1<\Delta f/f<1$, no defect modes of E or T_1 symmetry occur. Physically, this means that E and T_1 vibrations of the defect are strongly coupled to the bulk crystal so that these types of motion are not localized around the defect. The defect perturbation for E modes contains only bond-bending interactions which are relatively weak and produce defect modes only for $\Delta f/f\gg 1$. The defect perturbation for T_1 modes is identically zero as a result of rotational invariance and consequently no T_1 defect modes exist. The defect perturbation for A and T_2 modes contains bond-stretching and mass-defect terms which are relatively large and produce the modes shown here.

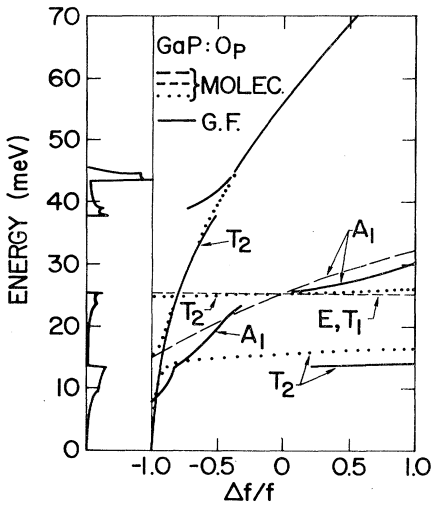

FIG. 5. Defect vibrational modes of oxygen on a P site in GaP. Energy of the modes is plotted vs the defect force constant $\Delta f/f$. Heavy solid lines show the solutions from the Green's-function calculations. Dashed and dotted lines give the vibrational modes of an OGa_4 molecule embedded in an immovable lattice. E and T_1 molecular modes are split by an amount too small to show in the figure. Bulk phonon DOS is shown on the left-hand side of the figure.

The energy of some Green's-function modes are quite close to those calculated from a simple molecular model. In Fig. 5 we show the modes for a OGa_4 molecule imbedded in an immovable lattice according to the formulas given in Appendix C. From the figure it is apparent that the A_1 molecular mode agrees very roughly with the A_1 Green's-function mode. Three T_2 molecular modes exist. Those modes near 25 meV are mainly T_2^a-type (bending motion of the Ga atoms perpendicular to the O—Ga bonds), those modes near 15 meV are mainly T_2^b type (stretching motion of the Ga atoms parallel to the O—Ga bonds), and the modes which vary quadratically with $\Delta f/f$ are mainly T_2^c type (O-atom motion). The modes have mixed nature near the crossing points of the branches. Some of the molecular results agree closely with the Green's-function modes, but other molecular modes appear where there are no Green's-function modes. In the latter case the vibration of the defect is strongly coupled to the bulk modes so that a peak in the LDOS does not appear. This illustrates the major deficiency of the molecular-model results—the number of modes is determined by the size of the cluster. The Green's-function method allows us to couple these modes to the rest of the crystal in order to see if they remain somewhat localized around the defect. The real importance of the molecular-model calculations is that they provide a good check on the Green's function results, since in certain limits the results from both methods agree quite well.

IV. DISCUSSION

The vibrational states of the neutral oxygen defect O^0 are seen in the electron-capture luminescence of Dean and Henry.[2] In this spectrum the zero-phonon line is forbidden so that the strong one-phonon replicas must involve T_2 phonons.[10] As shown in Fig. 2 of Dean and Henry's work vibrational modes involving oxygen motion are seen at 24.7 and 28.4 meV (resonances in the acoustic branch) and various phonon replicas are also seen in the optical branch. Since oxygen has a smaller mass than phosphorous, it is necessary to considerably reduce the O—Ga force constants relative to the bulk Ga—P force constants to produce such low-energy modes.[5,6] Comparing the experimental results with the theoretical T_2 modes shown in Fig. 4 we see that it is necessary to reduce the strength of the defect force constants to $\Delta f/f<-0.8$ to produce the resonance in the acoustic branch. In Fig. 6 we show the LDOS for T_2 modes using $\Delta f/f=-0.85$, and mass defects corresponding to ^{16}O and ^{18}O. The theory predicts one T_2 resonant mode centered at 21.9 meV for ^{16}O. Dean and Henry[2] report a value of -1.6 meV for the $^{16}O\rightarrow{}^{18}O$ isotope shift of the 24.7 meV peak. As shown in Fig. 6 we calculate a shift of -1.14 meV for this resonance peak, which we consider to be within experimental uncertainty of the observed -1.6 meV considering the limited resolution of the $^{16}O_{loc}$ peak in the data.[2] Thus we identify our computed 21.9-meV resonance with the observed 24.7-meV mode. Our computed isotope shift is 83% of what would be expected for motion of the O atom alone. Alternatively, the LDOS gives the composition of the T_2 resonance mode to be $0.05T_2^a+0.87T_2^b+0.87T_2^c$.

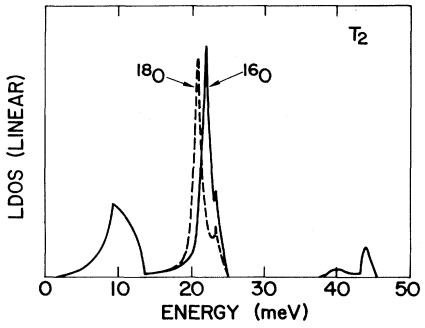

FIG. 6. LDOS for T_2 modes of ^{16}O (solid line) and ^{18}O (dashed line) defects using a defect force constant of $\Delta f/f=-0.85$.

According to our calculations the first-shell Ga atoms always make a significant contribution to the resonance. Motion of the O atom alone is not a normal mode of the system (except for $\Delta f/f=-1$).

The vibrational mode observed[2] at 28.4 meV is not well described by the present theory. However, we suggest that this feature is partly due to a peak in the bulk T_2 DOS (LA phonons) which adds structure to the LDOS. This feature does not appear in Fig. 6 because of the simplified model used for the bulk phonons, but better models[8,20] do indeed show a strong peak near 27 meV. In the optical branch the experiments observe a number of vibrational modes. In Fig. 6 we see some small features in the optical branch, but these are associated only with the bulk DOS and are not localized near the defect. However, as discussed above, the LO branch of our theoretical phonon dispersion curves is quite crude and more sophisticated models may produce additional defect modes there.

Phonons of energy 19.5 and 47 meV have been observed for the O^+ defect in the donor-acceptor—pair (DAP) luminescence of Dean, Henry, and Frosch.[1] Morgan[10] argues that these phonons are A_1-type modes since the zero-phonon transition is allowed. We note that phonons involving colinear motion of the oxygen and acceptor atoms are in fact allowed in the DAP spectra (these modes are T_2 type with respect to the T_d symmetry of the isolated O atom). This fact led us originally to conclude that the 47-meV phonon was a T_2 mode involving resonant O motion.[18] However, calculations show that the intensity of a strictly localized T_2 phonon replica in a DAP spectrum is very weak for distant DAP's. This probably is true for localized resonant modes also. We conclude that the 47-meV mode does not involve localized O motion.

In photoluminescence excitation experiments on the O^0 defect, Monemar and Samuelson[3] observed phonons of energy 19 and 48 meV. These energies equal those for the O^+ defect within an experimental uncertainty of about 5%. Alternatively, Henry and Lang[21] propose a shift of 22% in the phonon energies of the different charge states in order to explain observed nonradiative capture cross sections. These two results are not necessarily inconsistent since the 19- and 48-meV modes may be relatively insensitive to force-constant changes, whereas the capture—cross-section data include the T_2 modes which are quite dependent on the defect force constants. A good method to determine the difference between O^+ and O^0 force constants would be the observation of the O^+ T_2 mode, predicted by Baraff *et al.*[6] to lie at 32.4 meV. In any case, considering the accuracy of the computations present here, the difference between O^+ and O^0 force constants is relatively small and we will henceforth use the same force constants ($\Delta f/f=-0.85$ as determined above) for both charge states.

Turning now to the calculation, for $\Delta f/f=-0.85$ we find an A_1 resonance at 12.2 meV, which we identify with the observed 19-meV phonon. In the present model the computed energy of this mode is somewhat low, but results from more complicated models[9] yield an A_1 phonon energy much closer to that observed. The computed resonance has a width of about 5 meV, which is comparable to the 3-meV lifetime broadening estimated by Monemar and Samuelson.[3] The breadth of this resonance indicates that it is not too strongly localized around the defect, so that the mode involves breathing motion of the first Ga shell along with significant contributions from further shells. In the optical branch we find no A_1 resonances for $\Delta f/f\approx-0.85$. There are no A_1 modes here because optical phonons involve mainly P-atom motion (see Sec. III B), and in the present calculation it is very difficult to localize this type of motion since the P atoms are in the second shell around the O atom but the defect force constants extend only to the first shell. Possibly an A_1 mode in the optical branch could be produced by adjusting second-nearest-neighbor O—P bonds or Ga—P back bonds. However, from the present model we conclude that the 47-meV mode does not involve localized breathing motion of the first Ga shell.

In summary, for a defect force constant of $\Delta f/f=-0.85$ our theory finds an A_1 resonance at 12.2 meV and a T_2 resonance at 21.9 meV, which we identify with the observed 19.5- (Ref. 1) and 24.7-meV (Ref. 2) modes, respectively. No other defect modes are predicted by the theory and we conclude that other observed modes are not localized at the O impurity or in the first Ga shell. As discussed above, the identification by Morgan[10] of the observed 47-meV (Refs. 1 and 3) phonon as an A_1 mode localized on P atoms is consistent with our results. Also we argue that the observed 28.4-meV peak (Ref. 2) may be partly due to a peak in the LA-phonon bulk DOS. Similarly, the phonons labeled $A-C$ in the capture luminescence (Ref. 2) may also be due to peaks in the bulk DOS or they may be some type of delocalized vibrational modes of the defect.

V. CONCLUSIONS

In this paper we theoretically analyze the vibrational modes of substitutional oxygen in GaP using nearest-neighbor interactions only. Our theory predicts the presence of basically one mode of A_1 symmetry and one mode of T_2 symmetry which are localized (strictly localized or resonant) around the O impurity. We identify these localized modes with phonons observed in the optical spectra of the O^0 and O^+ defects, and we argue that other pho-

nons observed in these spectra are relatively delocalized. By the term delocalized, we mean a bulk phonon or a defect mode which is not significantly localized at the O impurity or in the first shell of Ga atoms. We should emphasize that the number of localized modes predicted by the present theory is largely determined by the model used for the defect perturbation, i.e., relaxation of nearest-neighbor O—Ga force constants only. More sophisticated defect models do produce additional localized modes, and these modes will be discussed in a forthcoming publication.[9] However, since the defect perturbation is basically unknown, we feel that even the simple results presented here provide new insight concerning the nature of the vibrational modes of oxygen in GaP.

ACKNOWLEDGMENTS

The authors thank T. N. Morgan for useful discussions. Valuable computation assistance was provided by C. A. Swarts. One of us (R.M.F.) was supported by a scholarship from the Natural Sciences and Engineering Research Council of Canada. This work was supported in part by the Office of Naval Research under Contract No. N00014-81-K-0305.

APPENDIX A: COLLECTIVE COORDINATES FOR A FIVE-ATOM TETRAHEDRAL CLUSTER

The collective coordinates Q are expressed in terms of the Cartesian coordinates (x,y,z) of each atom. The atoms are numbered 0—4 located along lattice directions (0,0,0), (1,1,1), $(-1,-1,1)$, $(-1,1-1)$, and $(1,-1,-1)$, respectively. The collective coordinates form bases for the irreducible representation of the T_d group as indicated. NF denotes the normalization factor.

	A_1	E		T_1			T_2^a			T_2^b			T_2^c		
	Q_1	Q_2	Q_3	Q_4	Q_5	Q_6	Q_7	Q_8	Q_9	Q_{10}	Q_{11}	Q_{12}	Q_{13}	Q_{14}	Q_{15}
x_0	0	0	0	0	0	0	0	0	0	0	0	0	1	0	0
y_0	0	0	0	0	0	0	0	0	0	0	0	0	0	1	0
z_0	0	0	0	0	0	0	0	0	0	0	0	0	0	0	1
x_1	1	−1	1	0	1	−1	2	−1	−1	1	1	1	0	0	0
y_1	1	−1	−1	−1	0	1	−1	2	−1	1	1	1	0	0	0
z_1	1	2	0	1	−1	0	−1	−1	2	1	1	1	0	0	0
x_2	−1	1	−1	0	1	1	2	−1	1	1	1	−1	0	0	0
y_2	−1	1	1	−1	0	−1	−1	2	1	1	1	−1	0	0	0
z_2	1	2	0	−1	1	0	1	1	2	−1	−1	1	0	0	0
x_3	−1	1	−1	0	−1	−1	2	1	−1	1	−1	1	0	0	0
y_3	1	−1	−1	1	0	−1	1	2	1	−1	1	−1	0	0	0
z_3	−1	−2	0	1	1	0	−1	1	2	1	−1	1	0	0	0
x_4	1	−1	1	0	−1	1	2	1	1	1	−1	−1	0	0	0
y_4	−1	1	1	1	0	1	1	2	−1	−1	1	1	0	0	0
z_4	−1	−2	0	−1	−1	0	1	−1	2	−1	1	1	0	0	0
NF	$\sqrt{12}$	$\sqrt{24}$	$\sqrt{8}$	$\sqrt{8}$	$\sqrt{8}$	$\sqrt{8}$	$\sqrt{24}$	$\sqrt{24}$	$\sqrt{24}$	$\sqrt{12}$	$\sqrt{12}$	$\sqrt{12}$	1	1	1

APPENDIX B: ELEMENTS OF THE DEFECT-PERTURBATION MATRIX δL USED FOR THE GREEN'S-FUNCTION COMPUTATIONS

The defect consists of a central O atom surrounded by four identical Ga atoms. The difference between the O—Ga force constants and those of the bulk is denoted Δf_1 for bond-stretching and Δf_2 for bond-bending interactions. The mass difference is denoted by $\Delta m = m_O - m_P$. Bond-bending interaction of strength μ are introduced between the Ga atoms and $\mu = -\Delta f_2/4$ by rotational invariance. The subscripts $a-c$ in the T_2 matrix refer to the collective coordinates listed in Appendix A. We write

$$\delta L(A_1)=\frac{1}{m_{\mathrm{Ga}}}\Delta f_1\ ,\quad \delta L(E)=\frac{1}{m_{\mathrm{Ga}}}(\Delta f_2+3\mu)\ ,\quad \delta L(T_1)=\frac{1}{m_{\mathrm{Ga}}}(\Delta f_2+4\mu)\ ,\quad \delta L_{aa}(T_2)=\frac{1}{m_{\mathrm{Ga}}}(\Delta f_2+\tfrac{2}{3}\mu)\ ,$$

$$\delta L_{bb}(T_2)=\frac{1}{m_{\mathrm{Ga}}}(\Delta f_1+\tfrac{4}{3}\mu)\ ,\quad \delta L_{cc}(T_2)=\frac{1}{m_{\mathrm{P}}}(\tfrac{4}{3}\Delta f_1+\tfrac{8}{3}\Delta f_2-\omega^2\Delta m)\ ,\quad \delta L_{ab}(T_2)=\delta L_{ab}(T_2)=-\frac{\sqrt{8}}{3m_{\mathrm{Ga}}}\mu\ ,$$

$$\delta L_{bc}(T_2)=\delta L_{cb}(T_2)=\left[\frac{4}{3m_{\mathrm{Ga}}m_{\mathrm{P}}}\right]^{1/2}\Delta f_1\ ,\quad \delta L_{ac}(T_2)=\delta L_{ca}(T_2)=\left[\frac{8}{3m_{\mathrm{Ga}}m_{\mathrm{P}}}\right]^{1/2}\Delta f_2\ .$$

APPENDIX C: VIBRATION FREQUENCIES ω OF AN OGa_4 CLUSTER EMBEDDED IN AN IMMOVABLE LATTICE

Nearest-neighbor bond-stretching and bond-bending force constants f_1' and f_2', respectively, refer to O—Ga bonds and f_1 and f_2 refer to those bonds connecting the Ga atoms to the immovable lattice. Second-nearest-neighbor bond-bending interactions of strength μ are introduced between the Ga atoms and $\mu=-(f_2'-f_2)/4$ by rotational invariance. The subscripts $a-c$ in matrix $\underline{C}$ refer to the collective coordinates listed in Appendix A. We have

$$\omega^2(A_1)=\frac{1}{m_{\mathrm{Ga}}}(f_1'+\tfrac{1}{3}f_1+\tfrac{8}{3}f_2),\quad \omega^2(E)=\frac{1}{m_{\mathrm{Ga}}}(f_2'+3\mu+\tfrac{4}{3}f_1+\tfrac{5}{3}f_2),\quad \omega^2(T_1)=\frac{1}{m_{\mathrm{Ga}}}(f_2'+4\mu+\tfrac{4}{3}f_1+\tfrac{5}{3}f_2)\ ,$$

$$\omega^2(T_2)=\text{ eigenvalues of matrix }\underline{C},\quad C_{11}=\frac{1}{m_{\mathrm{Ga}}}(f_2'+\tfrac{2}{3}\mu+\tfrac{4}{3}f_1+\tfrac{5}{3}f_2)\ ,\quad C_{22}=\frac{1}{m_{\mathrm{Ga}}}(f_1'+\tfrac{4}{3}\mu+\tfrac{1}{3}f_1+\tfrac{8}{3}f_2)\ ,$$

$$C_{33}=\frac{1}{m_{\mathrm{O}}}(\tfrac{4}{3}f_1'+\tfrac{8}{3}f_2'),\quad C_{12}=C_{21}=-\frac{\sqrt{8}}{3m_{\mathrm{Ga}}}\mu\ ,\quad C_{23}=C_{32}=\left[\frac{4}{3m_{\mathrm{Ga}}m_{\mathrm{O}}}\right]^{1/2}f_1',\quad C_{13}=C_{31}=\left[\frac{8}{3m_{\mathrm{Ga}}m_{\mathrm{O}}}\right]^{1/2}f_2'\ .$$

---

*Permanent address: IBM Thomas J. Watson Research Center, Yorktown Heights, NY 10598.

[1]P. J. Dean, C. H. Henry, and C. J. Frosch, Phys. Rev. 168, 812 (1968).

[2]P. J. Dean and C. H. Henry, Phys. Rev. 176, 928 (1968).

[3]B. Monemar and L. Samuelson, J. Lumin. 12/13, 507 (1976); Phys. Rev. B 18, 809 (1978).

[4]P. J. Dean, Physica 117&118B, 140 (1983).

[5]R. M. Feenstra and T. C. McGill, Phys. Rev. Lett. 47, 925 (1981).

[6]G. A. Baraff, E. O. Kane, and M. Schlüter, Phys. Rev. Lett. 47, 601 (1981); Phys. Rev. B 25, 548 (1982).

[7]A. Grimm, A. A. Maradudin, I. P. Ipatova, and A. V. Subashiev, J. Phys. Chem. Solids 33, 775 (1972).

[8]K. Kunc, Phys. Status Solidi B 72, 229 (1975); Ann. Phys. (Paris) 8, 319 (1973).

[9]R. J. Hauenstein, T. C. McGill, and R. M. Feenstra (unpublished).

[10]T. N. Morgan, Phys. Rev. Lett. 40, 190 (1968).

[11]A. A. Maradudin, Rep. Prog. Phys. 28, 331 (1965); in *Solid State Physics,* edited by F. Seitz and D. Turnbull (Academic, New York, 1966), Vol. 18, p. 273.

[12]D. N. Talwar, M. Vandevyver, and M. Zigone, J. Phys. C 13, 3775 (1980).

[13]J. deLaunay, in *Solid State Physics,* edited by F. Seitz and D. Turnbull (Academic, New York, 1956), Vol. 2, p. 210.

[14]J. Berholc, N. O. Lipari, and S. T. Pantelides, Phys. Rev. B 21, 3545 (1980).

[15]J. Bernholc and S. T. Pantelides, Phys. Rev. B 18, 1780 (1978).

[16]G. Gilat and L. J. Raubenheimer, Phys. Rev. 144, 390 (1966).

[17]J. F. Janak, in *Computational Methods in Band Theory,* edited by P. M. Marcus, J. F. Janak, and A. R. Williams (Plenum, New York, 1971), p. 323.

[18]R. M. Feenstra and T. C. McGill, Physica 117&118B, 149 (1983).

[19]P. J. Dean, Phys. Rev. 157, 655 (1967).

[20]J. L. Yarnell, J. L. Warren, R. G. Wenzel, and P. J. Dean, in *Neutron Inelastic Scattering* (IAEA, Vienna, 1968), Vol. 1, p. 301; see also Fig. 50 of A. S. Barker, Jr. and A. J. Sievers, Rev. Mod. Phys. 47, Suppl. 2 (1975).

[21]C. H. Henry and D. V. Lang, Phys. Rev. B 15, 989 (1977).